Molecular Sieves

DOI: 10.1002/ange.201003273

Unified Internal Architecture and Surface Barriers for Molecular Diffusion of Microporous Crystalline Aluminophosphates**

*Lukasz Karwacki, Hendrik E. van der Bij, Jan Kornatowski, Pablo Cubillas, Martyn R. Drury, D. A. Matthijs de Winter, Michael W. Anderson, and Bert M. Weckhuysen**

Microporous crystalline aluminophosphates, an important class of molecular sieves, are of great interest as adsorbents, membrane materials, and heterogeneous catalysts.[1–5] They are active in, for example, alkene isomerization, catalytic cracking, alkane dehydrogenation, and hydrocarbon oxidation.[6–11] To expand our understanding of transport mechanisms and diffusion in microporous crystalline aluminophosphates and connect this information to their catalytic and sorption properties, scientists have performed extensive research on large crystals as model systems.[12–16]

For about twenty years it has been known that the properties of large crystals are severely influenced by building defects. For example, Lehman et al.[17,18] elucidated the internal structure of CrAPO-5 molecular sieves by studying the intracrystalline concentration profiles of probe molecules such as methanol and water by interference and FTIR microscopy. They showed an inhomogeneous distribution of water adsorbed at low pressures in CrAPO-5 and SAPO-5 molecular sieves, attributed to structural defects in the crystals. This work was confirmed by Chmelik et al.,[19] who focused on the influence of surface and intracrystalline defects on molecular uptake.

[*] L. Karwacki, H. E. van der Bij, Prof. Dr. B. M. Weckhuysen
Inorganic Chemistry and Catalysis Group, Debye Institute for Nanomaterials Science, Faculty of Science, Utrecht University
Sorbonnelaan 16, 3584 CA Utrecht (The Netherlands)
Fax: (+31) 30-251-1027
E-mail: b.m.weckhuysen@uu.nl
Dr. J. Kornatowski
Max-Planck Institut für Kohlenforschung
45470 Mülheim/Ruhr (Germany)
and
Faculty of Chemistry, and Nicholas Copernicus University
87100 Torun (Poland)
Dr. P. Cubillas, Prof. Dr. M. W. Anderson
Centre for Nanoporous Materials, School of Chemistry
University of Manchester, Manchester M13 9LP (UK)
Dr. M. R. Drury
Department of Earth Sciences, Faculty of Geosciences
Utrecht University, 3508 TA Utrecht (The Netherlands)
D. A. M. de Winter
Biomolecular Imaging, Institute of Biomembranes
Faculty of Sciences, Utrecht University
3584 CH Utrecht (The Netherlands)

[**] We thank NWO for financial support (CW-NWO Top grant) and a large investment subsidy for the Dualbeam microscope. The authors thank M. Versluijs-Helder for the SEM measurements and A. M. Beale for fruitful discussion.

Supporting information for this article is available on the WWW under http://dx.doi.org/10.1002/anie.201003273.

Recently, we have developed confocal fluorescence microscopy (CFM) as a powerful method to study the internal architecture and molecular diffusion barriers of large crystals of molecular sieves through mapping of the template-removal process.[20,21] Thermal decomposition of the template molecules present in the channels and cages of the as-prepared materials leads to the formation of light-emitting and -absorbing species.[20] When fluorescent species diffuse through the channels and cages, transport resistances lead to different concentration profiles, which can be mapped in three dimensions with CFM.

The above-mentioned studies have proven that molecular sieves are not single-crystalline, but consist of distinct subunits forming inner and outer barriers that resist molecular diffusion.[16–22] Interestingly, the arrangement of these subunits, known as the internal architecture of a crystal, was found to be dependent not on the crystal framework type, but on the external morphology. For example, in the case of large MFI crystals (i.e., ZSM-5 and silicalite molecular sieves) it was found that four related but distinct intergrowth structures exist depending on the length/width (L/W) aspect ratios of the crystals.[21] On the other hand, two large AFI crystals, that is, CrAPO-5 and SAPO-5, exhibit different internal architectures, while seemingly having the same morphology.[20] This apparent contradiction merits thorough investigation.

Herein we present a systematic study on 8 micrometer-sized members of the AlPO-5 family with a wide range of morphologies and chemical composition. Confocal fluorescence microscopy (CFM), focused ion beam (FIB) milling, electron backscatter diffraction (EBSD), and atomic force microscopy (AFM) are used to gain new fundamental insight into the internal structure and molecular diffusion barriers of microporous crystalline aluminophosphates and to resolve the above-mentioned discrepancy in internal architectures of AFI-type materials. As a result, we are able to propose a unified AFI intergrowth structure.

Two groups of AFI crystals can be distinguished. On the one hand, we have investigated AlPO-5 crystals which contain Cr, V, or Si and grow with similar lengths of the a, b, and c axes, resulting in L/W ratios of approximately 1 and smaller (here denoted type A). On the other hand, MAPO-5 crystals (M = Zn, Be, Co, Cu and Mo) have a and b axes of similar length and a much longer c axis (two to seven times; type B). To gain insight into the internal architecture of the crystals, CFM scans of partially detemplated materials were taken at the middle depth of the crystals along the a/b and c axes. The results for the CrAPO-5 and MoAPO-5 crystals (showcasing crystal types A and B, respectively) are given in Figure 1a, while Figure S1 and Table S1 of the Supporting

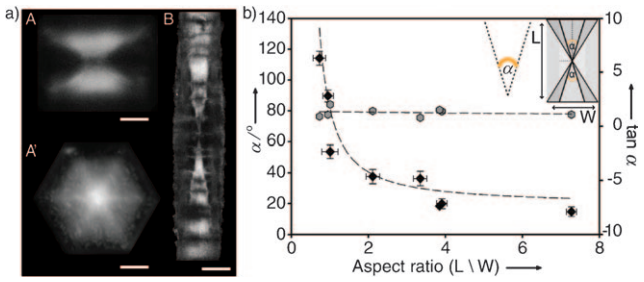

Figure 1. a) Confocal fluorescence images of CrAPO-5 (type A) and MoAPO-5 crystals (type B), recorded halfway through the crystal along the *a* axis for crystals A and B and along the *c* axis for crystal A′. Scale bar is 4 μm for crystal A and 50 μm for crystal B. The images are presented in grayscale; the brighter the image, the higher the fluorescence intensity. b) Relationship between the measured subunit angle (left axis) at different aspect ratios of MeAPO-5 crystals. The right axis is tan[$^1/_2\alpha/(L/W)$] and reveals a tangent dependency.

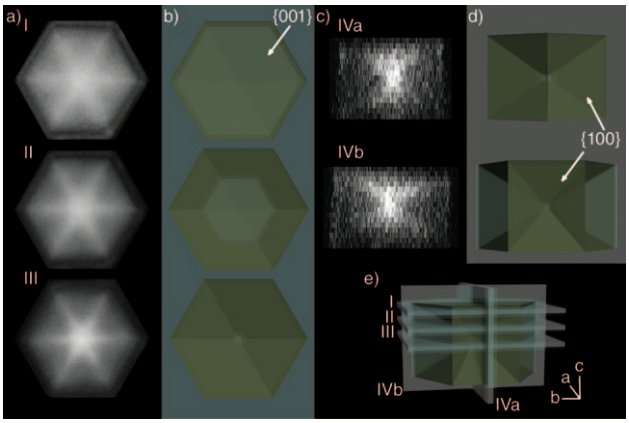

Figure 2. a) Confocal fluorescence images of an individual CrAPO-5 crystal. I, II, and III show slices through the crystal {001} face (along the *c* axis). b) Same as a), but based on the planar model of the internal structure of the CrAPO-5 crystal model. c) Data reconstructed in the *ac* and *bc* planes (planes IVa and IVb, respectively. d) Same as c), but for crystal planes visible along *a*/*b* axes (slices VIa and VIb, respectively). All rectangular faces are {100}. Images I–IV in b) and d) show simulated data of the different crystal planes and correlate with the planes recorded by confocal fluorescence microscopy in a) and c). e) Three-dimensional schematic representation of a CrAPO-5 crystal, showing the scanned crystal planes I–IV. Intensity of the fluorescent signal in layers I–III can be found in the Figure S2 in the Supporting Information.

Information give an overview of all materials studied. If we carefully examine the confocal fluorescence data collected from the crystals along the *a* axis, it is clear that all materials show an hourglass pattern, that is, they have the same internal structure comprising two hexagonal-based pyramids and six surrounding subunits. Interestingly, inspection of the CrAPO-5 crystal standing on its hexagonal base allowed us to obtain confocal information along the *c* axis showing a starlike pattern originating from the center of the crystal (crystal A′ in Figure 1a), as discussed in various studies.[16–22] The second, pyramid-shaped intergrowth observed in the crystals along the *a* axis was noted in elongated SAPO-5 and is similar to that found for the other framework types, for example, CHA and MFI.[20,22]

Our previous study on large MFI crystals[21] showed direct dependence of the internal structure on the external morphology of the crystal. To evaluate the presence of the above-mentioned dependency, the relationship between the *L*/*W* ratio of the MeAPO-5 crystals and the size (angle) of the subunits is plotted in Figure 1b. As visualized, the dependence of subunit angles on the crystal's aspect ratio follows the basic, trigonometric relation between crystal morphology and internal architecture, which at least suggests a uniform internal structure of all AFI-type materials.

To reveal the nature and the origin of the starlike pattern observed by CFM, confocal fluorescence data collected along the *c* axis of the CrAPO-5 crystal (parallel to the {001} crystal face) were analyzed (Figure 2). The high-resolution images collected on the different layers of the crystal revealed significant differences in the concentration of the fluorescent molecules, as the fluorescence intensity in the central part of the *ab* crystal plane increases with increasing crystal depth. Figure 2b shows the planar model of the internal structure of the CrAPO-5 crystal, expected to exist on the basis of the reconstruction of the CFM data. Planes dividing the six surrounding subunits appear as barriers, similar to the "star" visualized in Figure 2a. This similarity is further supported by the reconstructed confocal images and simulated data of the *ac* and *bc* planes, as shown in Figure 2c and d, respectively. Since the resolution of confocal fluorescence microscopy (see Figure S3 of the Supporting Information for CFM scheme) in the *c* direction is limited (in the best case) to about 1.2 μm, every scanned layer includes signal originating from the "out-of-focus" planes. The direct consequence of the above-mentioned limitation is a blurred image of the star-shaped pattern at layer I of the CrAPO-5 crystal (Figure 2a).

Until now, CFM allowed us to visualize the diffusion barriers of the AFI crystals under investigation, but it did not give us any information about the pore alignments in the distinct subcrystals and true internal crystal structure. To obtain such information, two different CrAPO-5 crystals were milled halfway through their thickness with a focused ion beam (FIB). A schematic illustration of the milled planes is given in Figure 3a. Next, EBSD patterns were recorded across the crystal surfaces. Strikingly, all of the recorded EBSD patterns within the individual plane show similar crystallographic orientation (Figure 3b). As the angular resolution of EBSD is on the order of 2°, we can say for certain that CrAPO-5 crystals do not have any high-angle rotational intergrowth, and therefore the presence of the starlike subcrystal should be indisputably excluded. Figure 3c shows an example of the manually indexed EBSD patterns, collected from the areas marked by violet and blue squares in Figure 3b. Importantly, manual indexing allowed us to assign the channel direction as parallel to the crystal long *c* axis. Crucially, no 60° rotation of the crystal subunits was measured, and this confirms the lack of high-angle rotation barriers.[21] To prove the uniformity of the proposed internal structure of the AFI-type materials, in the second set of FIB/EBSD experiments, a CoAPO-5 crystal was milled, and no intergrowth was evident (Figure S5, Supporting Information).

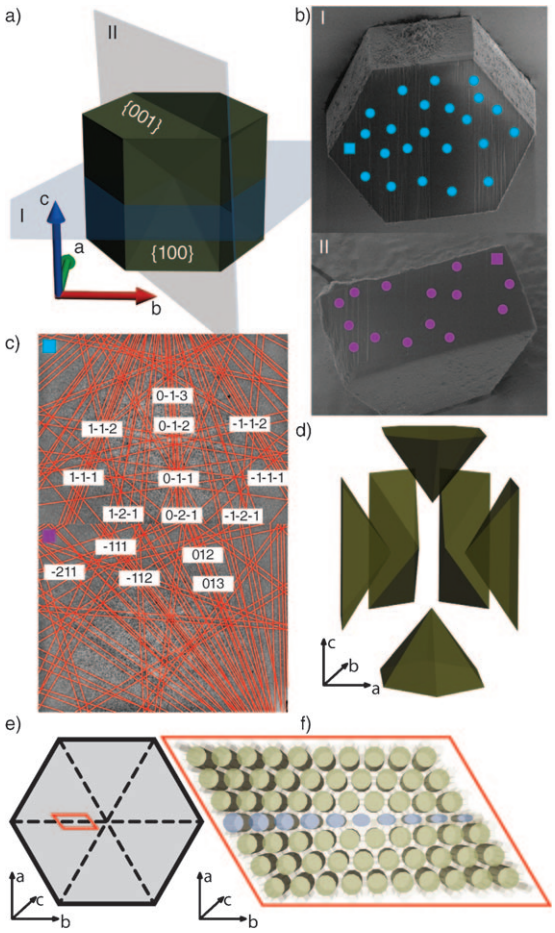

Figure 3. a) Three-dimensional representation of a CrAPO-5 crystal. Surfaces I and II indicate planes according to which crystals were milled (parallel to crystal {001} and {100} faces, respectively). Axes *a*, *b*, and c are known thanks to manual indexing of the diffraction patterns. b) SEM images of the CrAPO-5 crystals after FIB treatment according to the planes indicated in a). Regions from which diffraction patterns have been recorded are indicated by violet and blue circles. c) Two examples of the distinct, manually indexed diffraction patterns, recorded from the areas marked by violet and blue squares on planes I and II in b). d) "Exploded" unified internal architecture model of the AFI-type crystals; front subunits are not shown. e) Schematic visualization of the low-angle diffusion barriers (dashed lines) present in the hexagonal plane of the AFI-type crystals. f) Zoomed-in low-angle diffusion barrier present in the hexagonal plane of the AFI-type crystals. Small-angle framework rotation causes partial channel overlap and hinders molecular transport.

The starlike pattern found previously by Lehmann et al. and Chmelik et al. was assigned to the CrAPO-5 subcrystal.[17–19] The EBSD measurements, however, unambiguously prove the absence of high-angle rotation barriers, and hence different subunits in the "classical" understanding of zeolitic intergrowth,[21] and allow us to propose a uniform model of the AFI-type structure (Figure 3d). The origin of the starlike appearance is "simply" the presence of low-angle rotation diffusion barriers within the material. Planes where the steps from different faces meet generate small channel mismatches and a higher concentration of defects, which may act as a diffusion barrier. Figure 3e and f illustrate the schematic explanation of the low-angle diffusion barriers on the hexagonal plane of the crystal. There we can see that certain channels are partially blocked, hindering molecular diffusion of, for example, products of the template decomposition reaction, which accumulate on the interfaces of the hexagonal plane and lead to the appearance of the star-shaped pattern. In a similar manner, Figure S6 of the Supporting Information explains the presence of the hourglass pattern visible on the rectangular planes of both crystal types.

Being aware of the internal boundaries and differences in the crystals' aspect ratios, we should also expect significant differences in their external surface topography. Consequently, showcases of crystal type A (SAPO-5) and B (CoAPO-5) have been studied in detail with AFM (Figure 4; see Figure S7a of the Supporting Information for AFM data of all MeAPO-5 crystals).

Remarkably, as visualized in Figure 4a–d, crystals with an aspect ratio smaller than unity show curved steps on their

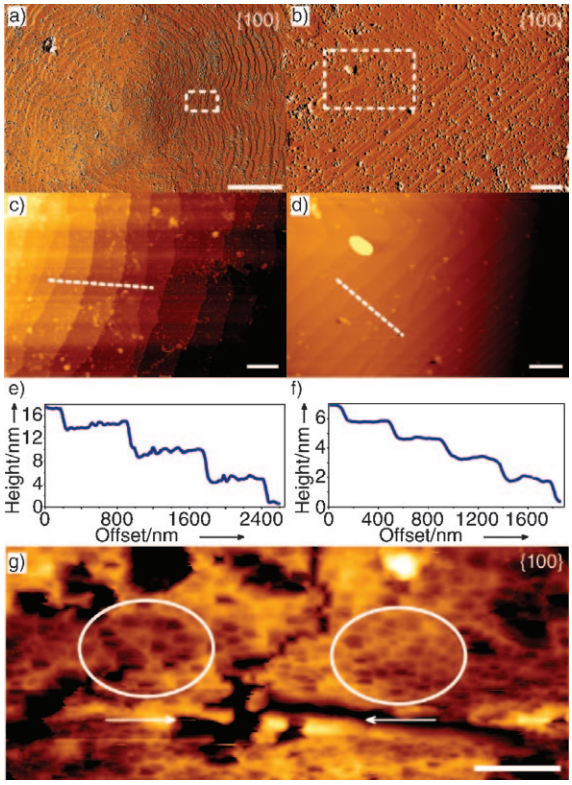

Figure 4. a) AFM image of a SAPO-5 crystal (type A); scale bar is 10 μm. b) Same as a), but for CoAPO-5 crystal (type B); scale bar is 2 μm. c) Enlarged AFM height image [indicated as a dashed rectangle in a)] recorded on the rectangular faces of the crystal; scale bar is 1 μm. d) Same as c), but for CoAPO-5. e) Measured step height along the white line in d), from left to right; the individual steps are bunched together and were determined to be about 2.4 nm and about 3.6 nm in height, that is approximately twice and three times the height of the monolayer of the hexagonal cell in the *ab* plane. f) Same as e), but for CoAPO-5; the analysis of the surface height reveals only monolayer steps of about 1.2 nm. g) An AFM height image of the central area of the MoAPO-5 crystal surface exhibiting dissolution etch pits pointing in opposite directions and divided by the small "crack" going from the top of the image to the bottom. Scale bar is 0.6 μm. All AFM images were recorded on crystal {100} faces.

surfaces, whereas those with a higher aspect ratio have straight steps. In both cases steps are generated by the presence of a spiral, but in the case of type A crystal steps bunch together (Figure 4e). On the contrary, the height analysis of the surface of type B crystals reveals only steps of monolayer height, that is, 1.2 ± 0.05 nm (Figure 4f). This height is consistent with the length of the *a*/*b* axes (or d_{100} spacing) of the hexagonal cell (ca. 1.2 nm); therefore, it can be unequivocally concluded that the crystals are bound by {100} faces and not by {110}, which could yield the same external morphology. Importantly, the step height is consistent in all facets studied, as expected from the EBSD experiment and internal structure model.

A careful analysis of the etch-pit shapes on the type B crystals provides more insight into the internal structure of the MeAPOs. As highlighted in Figure 4g, a large MoAPO-5 crystal exhibits two opposite orientations of the etch pits, which are very close to each other and separated by an irregular line running through the center of the crystal, that is, mirror plane. This is in accordance with the internal symmetry of the AFI-type crystals, in which no mirror or glide plane is perpendicular to the *c* axis but one exists parallel to it.

This behavior can be seen more clearly in Figure S7b–e (Supporting Information) and it was observed in all AFI crystals with an aspect ratio higher than unity, for which steps could be seen by AFM. Additionally, each specific orientation is always observed only in one half of the crystal. This leads to the conclusion that the crystals are in fact twinned, with the twin plane parallel to the {001} face and located approximately at the center of the crystal. Such twinning in AlPO-5 crystals has been reported previously[23] and its occurrence has been linked to the strong preference for growth along a particular direction. Interestingly, the twin plane does not act as a transport barrier and therefore was not detected by the confocal fluorescence experiments. This means that the "connection" between the twins is almost perfect and therefore forces a reflection twin with an identical EBSD pattern. The mechanism of a formation of the twin plane is most probably related to the formation of the P–P bonds across a (001) plane and driven by the preferential growth of the crystals in a specific direction, as explained in Figure S8 of the Supporting Information.

Although the effect of morphology on the internal architecture (size of the subunits) has become clear from other studies,[21] the effect of metal framework atoms is indirect. It was established that the use of metal ions during synthesis can force the templating molecules into alternative conformations that lead to different framework types, as recently shown by in situ Raman spectroscopy.[24] Secondly, several characterization studies confirmed that the use of Si^{4+} and Cr^{3+} during synthesis inhibits crystal growth along the *c* direction and thus results in low aspect ratios.[25–27] Our observations suggest that while certain metal ions affect the crystallization kinetics by inhibiting crystal growth rate along the *c* direction, other metal ions, such as Mo^{6+}, induce the opposite effect by promoting crystal growth in the *c* direction and forming very elongated crystals.

Our work connects the dependency of crystal morphology with the internal architecture, and proves that diffusion boundaries follow basic trigonometry and are identical throughout the population of large AFI crystals studied. A correlative characterization of various micrometer-sized MeAPO-5 molecular sieves, based on CFM, FIB-EBSD, and AFM, led to a unified view on AFI intergrowth architecture. The size of crystal subcomponents varies in a regular order in all materials, while the surface becomes more organized and rougher and has an influence on the molecular penetration. The presence of small-angle rotation barriers and rotation planes result in significant hindrance of molecular diffusion. The present data, together with those recently published for large MFI crystals,[21] convincingly show that CFM is a very sensitive and fast tool to detect both low and high rotation barriers to molecular diffusion. On the other hand, when details on the precise origin of these molecular diffusion barriers are needed, clearly more advanced, but time-consuming FIB-EBSD measurements are required.

Received: May 30, 2010
Published online: August 16, 2010

Keywords: confocal microscopy · crystal intergrowth · microporous materials · structure elucidation · zeolites

[1] J. M. Bennett, J. P. Cohen, E. M. Flanigen, J. J. Pluth, J. V. Smith, *ACS Symp. Ser.* **1983**, *218*, 109.
[2] J. M. Thomas, R. Raja, G. Sankar, R. G. Bell, *Nature* **1999**, *398*, 227.
[3] B. M. Weckhuysen, R. R. Rao, J. A. Martens, R. A. Schoonheydt, *Eur. J. Inorg. Chem.* **1999**, 565.
[4] M. Hartmann, L. Kevan, *Chem. Rev.* **1999**, *99*, 635.
[5] M. E. Davis, *Nature* **2002**, *417*, 813.
[6] J. Meusinger, H. Vinek, J. A. Lercher, *J. Mol. Catal.* **1994**, *87*, 263.
[7] B. Parlitz, E. Schreier, H. L. Zubowa, R. Eckelt, E. Lieske, G. Lischke, R. Fricke, *J. Catal.* **1995**, *155*, 1.
[8] D. L. Vanoppen, D. E. De Vos, M. J. Genet, P. G. Rouxhet, P. A. Jacobs, *Angew. Chem.* **1995**, *107*, 637; *Angew. Chem. Int. Ed. Engl.* **1995**, *34*, 560.
[9] M. Hartmann, S. Ernst, *Angew. Chem.* **2000**, *112*, 916; *Angew. Chem. Int. Ed.* **2000**, *39*, 888.
[10] J. M. Thomas, R. Raja, G. Sankar, R. G. Bell, *Acc. Chem. Res.* **2001**, *34*, 191.
[11] S. O. Lee, R. Raja, K. D. M. Harris, J. M. Thomas, B. F. G. Johnson, G. Sankar, *Angew. Chem.* **2003**, *115*, 1558; *Angew. Chem. Int. Ed.* **2003**, *42*, 1520.
[12] B. M. Weckhuysen, *Angew. Chem.* **2009**, *121*, 5008; *Angew. Chem. Int. Ed.* **2009**, *48*, 4910.
[13] J. Kärger, P. Kortunov, S. Vasenkov, L. Heinke, D. B. Shah, R. A. Rakoczy, Y. Traa, J. Weitkamp, *Angew. Chem.* **2006**, *118*, 8010; *Angew. Chem. Int. Ed.* **2006**, *45*, 7846.
[14] M. H. F. Kox, E. Stavitski, B. M. Weckhuysen, *Angew. Chem.* **2007**, *119*, 3726; *Angew. Chem. Int. Ed.* **2007**, *46*, 3652.
[15] E. Stavitski, M. R. Drury, D. A. M. de Winter, M. H. F. Kox, B. M. Weckhuysen, *Angew. Chem.* **2008**, *120*, 5719; *Angew. Chem. Int. Ed.* **2008**, *47*, 5637.
[16] D. G. Hay, H. Jaeger, K. G. Wilshier, *Zeolites* **1990**, *10*, 571.
[17] E. Lehmann, C. Chmelik, H. Scheidt, S. Vasenkov, B. Staudte, J. Karger, F. Kremer, G. Zadrozna, J. Kornatowski, *J. Am. Chem. Soc.* **2002**, *124*, 8690.
[18] E. Lehmann, S. Vasenkov, J. Karger, G. Zadrozna, J. Kornatowski, O. Weiss, F. Schuth, *J. Phys. Chem. B* **2003**, *107*, 4685.

[19] C. Chmelik, P. Kortunov, S. Vasenkov, J. Karger, *Adsorpt. J. Int. Adsorpt. Soc.* **2005**, *11*, 455.
[20] L. Karwacki, E. Stavitski, M. H. F. Kox, J. Kornatowski, B. M. Weckhuysen, *Angew. Chem.* **2007**, *119*, 7366; *Angew. Chem. Int. Ed.* **2007**, *46*, 7228.
[21] L. Karwacki, M. H. F. Kox, D. A. M. de Winter, M. R. Drury, J. D. Meeldijk, E. Stavitski, W. Schmidt, M. Mertens, P. Cubillas, N. John, A. Chan, N. Kahn, S. R. Bare, M. Anderson, J. Kornatowski, B. M. Weckhuysen, *Nat. Mater.* **2009**, *8*, 959.
[22] M. H. F. Kox, E. Stavitski, J. C. Groen, J. Perez-Ramirez, F. Kapteijn, B. M. Weckhuysen, *Chem. Eur. J.* **2008**, *14*, 1718.
[23] G. J. Klap, M. Wubbenhorst, J. C. Jansen, H. van Koningsveld, H. van Bekkum, J. van Turnhout, *Chem. Mater.* **1999**, *11*, 3497.
[24] M. G. O'Brien, A. M. Beale, C. R. A. Catlow, B. M. Weckhuysen, *J. Am. Chem. Soc.* **2006**, *128*, 11744.
[25] J. Kornatowski, G. Zadrozna, M. Rozwadowski, B. Zibrowius, F. Marlow, J. A. Lercher, *Chem. Mater.* **2001**, *13*, 4447.
[26] E. C. Van Steen, L. H. Claeys, *Stud. Surf. Sci. Catal.* **2004**, *154*, 1282.
[27] S. A. Schunk, D. G. Demuth, B. Schulz-Dobrick, K. K. Unger, F. Schuth, *Microporous Mesoporous Mater.* **1996**, *6*, 273.

